The Invisible Z' at the LHC

Frank J. Petriello, Seth Quackenbush, Kathryn M. Zurek

Physics Department, University of Wisconsin, Madison, WI 53706

frankjp@physics.wisc.edu, squackenbush@wisc.edu, kzurek@wisc.edu

Abstract

We study the feasibility of observing an invisibly decaying Z' at the LHC through the process $pp \to ZZ' \to \ell^+\ell^- XX^\dagger$, where X is any neutral, (quasi-) stable particle, whether a Standard Model (SM) neutrino or a new state. The measurement of the invisible width through this process facilitates both a model independent measurement of $\Gamma_{Z'\to\bar{\nu}\nu}$ and potentially detection of light neutral hidden states. Such particles appear in many models where the Z' is a messenger to a hidden sector, and also if dark matter is charged under the $U(1)'$ of the Z'. We find that with as few as 30 fb^{-1} of data the invisibly decaying Z' can be observed at 5σ over SM background for a 1 TeV Z' with reasonable couplings. If the Z' does not couple to leptons and therefore cannot be observed in the Drell-Yan channel, this process becomes a discovery mode. For reasonable hidden sector couplings, masses up to 2 TeV can be probed at the LHC. If the Z' does couple to leptons, then the rate for this invisible decay is predicted by on-peak data and the presence of additional hidden states can be searched for. With 100fb^{-1} of data, the presence of excess decays to hidden states can be excluded at 95% C.L. if they comprise 20-30% of the total invisible cross section.

1 Introduction

New massive $U(1)$ gauge bosons appear in numerous theories of physics beyond the Standard Model (SM). They appear in grand unified theories such as $SO(10)$ [1] and $E(6)$ [2], in theories of extra space-time dimensions as Kaluza-Klein excitations of the SM gauge bosons [3], and in Little Higgs theories of the electroweak sector [4]. Z' bosons that decay to leptons have a simple, clean experimental signature, and consequently can be searched for up to high masses at colliders. Current direct search limits from Tevatron experiments restrict the Z' mass to be greater than about 900 GeV when its couplings to SM fermions are identical to those of the Z boson [5]. The LHC experiments are expected to extend the Z' mass reach to more than 5 TeV [6].

Since the Z' signature is clean and its QCD uncertainties are small, it is likely that the couplings of a discovered Z' can be studied with reasonable accuracy to probe the high scale theory that gave rise to it. Many studies of how to measure Z' properties and couplings to SM particles have been performed [7]. A recent study performed a next-to-leading order QCD analysis of Z' properties at the LHC accounting for statistical, residual scale, and parton distribution error estimates, and concluded that four generation independent combinations of Z' couplings could be extracted at the LHC by making full use of available on-peak differential spectra [8] (another recent study on searching for the Z' is found in [9]). However, a degeneracy between quark and lepton couplings can not be removed by studying Z' bosons in the Drell-Yan channel; all observables in this mode are unchanged if the quark couplings are scaled by a factor x while the lepton couplings are scaled by $1/x$. A different production mechanism must be utilized to remove this degeneracy. Possibilities are $pp \to Z' \to jj, b\bar{b}$, and $t\bar{t}$; however, because of SM backgrounds, all three are expected to be extremely difficult to observe at the LHC [10].

Another possible way of removing this degeneracy is by using the Z' width. The width takes the form

$$\Gamma = \Gamma_{inv} + \Gamma_{oth} + \sum_q \Gamma_q + \sum_l \Gamma_l. \tag{1.1}$$

Γ_{inv} is the partial width for Z' decays into invisible states such as SM neutrinos, Γ_q and Γ_l denote the widths for Z' decays into quarks and leptons respectively, and Γ_{oth} represents possible other decay modes such as $Z' \to W^+W^-, Zh$. This relation does not suffer from the same degeneracy as noted above. The total width Γ can be measured by fitting the shape of the resonance peak assuming the Z' is not too narrow. Γ_{oth} is small for large classes of models. If we make the mild theoretical assumption that $SU(2)_L$ invariance equates the Z' couplings of charged leptons to those of neutrinos (satisfied in grand unified models), and note that the on-peak study of [8] showed that the combination $c_q \sim \Gamma_q\Gamma_l/\Gamma^2$ can be measured, Eq. (1.1) becomes a quadratic equation for the unknown Γ_q, Γ_l that can be solved up to a two-fold discrete ambiguity. The only other assumption entering this procedure is that Γ_{inv} is composed entirely of Z' decays to neutrinos.

Besides breaking this degeneracy between quark and lepton couplings, there is an additional strong motivation for studying the invisible width of the Z'. Z' bosons often appear as messengers which connect the SM to hidden sectors, such as in some models of supersym-

metry breaking [11] and in Hidden Valley models [12], and can decay to light particles in this hidden sector. For example, Hidden Valley models contain sub-TeV mass states which are electrically neutral and quasi-stable, with decay lengths in some cases longer than tens of meters. These exit the detector as missing energy. A sterile neutrino which is charged under the $U(1)'$ would also result in hidden decays of the Z'. Such states may also account for the observed dark matter, as in the model of [13]. A model of milli-charged dark matter from a Stueckelberg Z' may also be found in Ref. [14].

In this paper we study whether invisible decays of the Z' can be detected at the LHC using the channel $pp \to ZZ' \to \ell^+\ell^- \not{E}_T$. This mode has previously been used to search for invisible decays of the Higgs boson [15]. As we will be interested in the large missing E_T kinematic region, $\not{E}_T \sim 200$ GeV, the experimental signature is relatively clean. Other possible channels such as $pp \to \gamma \not{E}_T, j \not{E}_T$ are sensitive to significant uncertainties such as jet energy mismeasurements and jets faking photons. We demonstrate that invisible Z' decays can be seen over the SM background with a significance of $S/\sqrt{B} = 3$ with as little as $10\,\text{fb}^{-1}$ for realistic models, while $S/\sqrt{B} = 5$ can be obtained with $30\,\text{fb}^{-1}$. We show that the structure of the $pp \to ZZ' \to \ell^+\ell^- \not{E}_T$ cross section admits a simple parametrization using two effective charges, associated with emission of the Z boson from either intitial state quarks or final state neutrinos. This allows invisible Z' decays to be studied in a model-independent fashion. For hidden sector states, only the initial state radiation contribution occurs. Assuming that the only invisible decays of the Z' are to SM neutrinos, these charges are predicted by the Drell-Yan study in [8]. Any deviation would indicate Z' couplings to light hidden sector states. We quantify what deviations can be seen given expected errors. We find that hidden sector decays making up 20-30% of the total invisible width can be observed at the LHC. If the Z' does not couple to leptons but decays to hidden sector states, $pp \to ZZ' \to \ell^+\ell^- \not{E}_T$ becomes a discovery mode. We show that leptophobic Z' bosons with masses up to 2 TeV can be probed at the LHC. With an integrated luminosity of $100\,\text{fb}^{-1}$, one can exclude a pure hidden sector Z' with $\sigma_{hid} > 0.3$ fb with a confidence of 95%; for $1000\,\text{fb}^{-1}$, one can exclude decays to hidden sector states down to 0.1 fb. A 3σ discovery can be achieved with $\sigma_{hid} > 0.6$ fb for $100\,\text{fb}^{-1}$, and $\sigma_{hid} > 0.2$ fb for $1000\,\text{fb}^{-1}$. We interpret these results in terms of the introduced effective charges.

Our paper is organized as follows. In Section 2 we explain our choice of invisible decay channel, and discuss backgrounds. In Section 3, we subject signal and background to cuts to isolate invisible decays, and parametrize the cross section in terms of Z initial state radiation (ISR) and final state radiation (FSR) contributions; hidden decays, which do not couple to the Standard Model, only appear in ISR contributions. We examine typical masses and couplings that can be probed, as well as kinematic differences between ISR and FSR. In Section 4 we determine whether decays to hidden sector states can be determined apart from SM neutrinos, using predictions from on-peak data as a background. Finally, we conclude in Section 5.

2 Signal and backgrounds

We begin by explaining how we search for invisible Z' decays. We focus on the channel $pp \to ZZ' \to \ell^+\ell^- \not{E}_T$, where $\ell = e, \mu$. Other possible signal processes to consider are $pp \to \gamma Z' \to \gamma \not{E}_T$ and $pp \to jZ' \to j\not{E}_T$. These, however, are more sensitive to uncertainties such as jet energy mismeasurements and jets faking photons. They require a detailed simulation beyond the scope of our analysis. We impose the following basic acceptance cuts on the two leptons in our signal: $|\eta_\ell| < 2.5$, $\Delta R_{\ell\ell} > 0.4$, and $p_T^\ell > 10\,\text{GeV}$. We compute the signal using MadEvent [17]; unless noted otherwise, we use MadEvent for all signal and background calculations.

The dominant Standard Model backgrounds to our signal fall into two categories: the production of leptons and neutrinos without a Z' in the intermediate state, and the production of Z + jets where the jets escape down the beam-pipe or have their energies mismeasured. We first consider SM production of leptons and neutrinos, $pp \to \ell^+\ell^-\nu\bar{\nu}$. We compute the full SM background with all interference effects and spin correlations included. The primary subprocesses contributing to this background are $pp \to W^+W^- \to \ell^+\ell^-\nu\bar{\nu}$ and $pp \to ZZ \to \ell^+\ell^-\nu\bar{\nu}$. We reduce the WW background using an invariant mass cut on the two leptons: $m_Z - 10\text{ GeV} < m_{\ell\ell} < m_Z + 10\text{ GeV}$. This restriction helps, but the WW background is still significant. Further reduction of this and the ZZ background is obtained by a $\not{E}_T$ cut, which we discuss in detail later. Other kinematic properties, such as the $\Delta\phi$ separation between the two leptons in our signal, do not significantly help once the $\not{E}_T$ cut is imposed.

We must also discuss the potentially large background $pp \to Z$ + jets, where the jets escape detection and fake a source of missing E_T. The LHC hadron calorimeters have a very wide rapidity coverage, up to $\eta \sim 4.9$, but soft jets in the central region are difficult to measure. We therefore restrict ourselves to vetoing jets with $p_T > 50$ GeV in the central region. Many soft jets may add up to substantial missing E_T; this can be a problem since the Z cross section is so large to begin with.

We perform a crude estimate of the two possible sources of Z + jets background: jets escaping down the beam-pipe or soft jets in the central region. We anticipate in this analysis the missing E_T cuts we will later impose to study 1-2 TeV Z' bosons, $\not{E}_T > 150 - 200\,\text{GeV}$. We begin by estimating the cross section for a hard jet with $p_T > 50$ GeV to escape down the beam-pipe. Using MadEvent we find 81 ab for $\not{E}_T > 100$ GeV and 29 ab for $\not{E}_T > 200$ GeV. These are very small compared to other backgrounds and will be neglected later in our study. For softer jets, in order to achieve enough missing E_T, it will take more (and potentially softer) jets than MadEvent can handle. We roughly estimate this background in the following way. We require a Z boson and at least one hard jet with $p_T > 30$ GeV in MadEvent. This cross section is ~ 334 pb. The resulting events are then showered using Pythia [18]. The surviving cross section drops off rapidly with a missing E_T cut:~ 690 ab remains after a cut of $\not{E}_T > 150$ GeV, and $\lesssim 50$ ab (no generated events remain) after $\not{E}_T > 200$ GeV. We require $\not{E}_T > 150$ GeV in our analysis, even when a smaller cut would be optimal for the neutrino background, to avoid the Z + jets background. At this point the background is dominated by the neutrino component, and Z + jets can be dropped

for statistical purposes. However, an analysis should be performed once Z + jets can be determined more precisely.

All signal and background processes in our study are calculated at leading order in the QCD perturbative expansion using a running scale for α_s. The next-to-leading order corrections to the background processes are known [19], while the corrections to the signal process are easily calculable. Since we later use as our significance estimator the ratio of signal over background fluctuation, $S/\sqrt{B}$, we feel this is a conservative approach; including the K-factors for both S and B would improve our results. We note that the dependence of the next-to-leading order cross section on the renormalization and factorization scales indicates that uncertainties arising from uncalculated higher order corrections are at the few percent level or less. In most of our analysis we also neglect errors associated with imprecise knowledge of parton distribution functions. For the gauge boson production processes considered here, it is likely that LHC data can determine these to high accuracy. The analysis in Ref. [20] indicates that the parton distribution function errors for di-boson process such as the $pp \to WW, ZZ$ backgrounds considered here may be reduced to the percent level by normalizing their rates to the LHC Drell-Yan data samples. Detector effects such as smearing were determined to have a small effect on lepton distributions in [16], and we neglect them in our analysis as well. We neglect other detector issues such as smearing of the $\not{E}_T$ distributions caused by un-vetoed soft jets and the underlying event; although we expect them to be relatively unimportant due to our large missing E_T cut, they are difficult to estimate with current tools. These issues should be revisited in a more complete study which makes use of LHC data, but we believe their neglect is justified in this initial analysis.

3 Studying the invisible Z'

Employing the cuts and techniques described in the previous section, we determine whether invisible Z' decays can be observed over the SM background. We map out the missing E_T dependence in Figs. (1) and (2). The basic cuts outlined in the previous section have been implemented. Both plots show the SM background $pp \to \ell^+\ell^-\nu\bar{\nu}$ as a function of a lower cut on the missing E_T. Two fiducial models are also shown: the sequential Standard Model and the $U(1)_\chi$ model with an overall gauge coupling $g' = 1$. We assume $M_{Z'} = 1$ TeV for both models. The plots begin at $\not{E}_T = 100$ GeV to avoid serious issues with the Z + jets background. We also plot the required invisible Z' cross sections for observation at the LHC assuming $10\,\text{fb}^{-1}$, $30\,\text{fb}^{-1}$, and $100\,\text{fb}^{-1}$. Fig. (1) shows the required cross section for a statistical significance of $S/\sqrt{B} = 5$, while Fig. (2) shows the required rate for $S/\sqrt{B} = 3$. Two facts can be observed from these graphs. First, the optimum missing E_T cut for TeV mass Z' bosons is around 200 GeV, above the level where Z + jets is a serious concern. Second, for realistic models a signal is observable at the LHC even with moderate integrated luminosity. $S/\sqrt{B} = 3$ is possible for both fiducial models with less than $30\,\text{fb}^{-1}$, while $S/\sqrt{B} = 5$ is possible for less than $100\,\text{fb}^{-1}$.

We wish to do more than simply observe the invisibly decaying Z'. We also want to measure the underlying parameters leading to these decays, and determine whether the

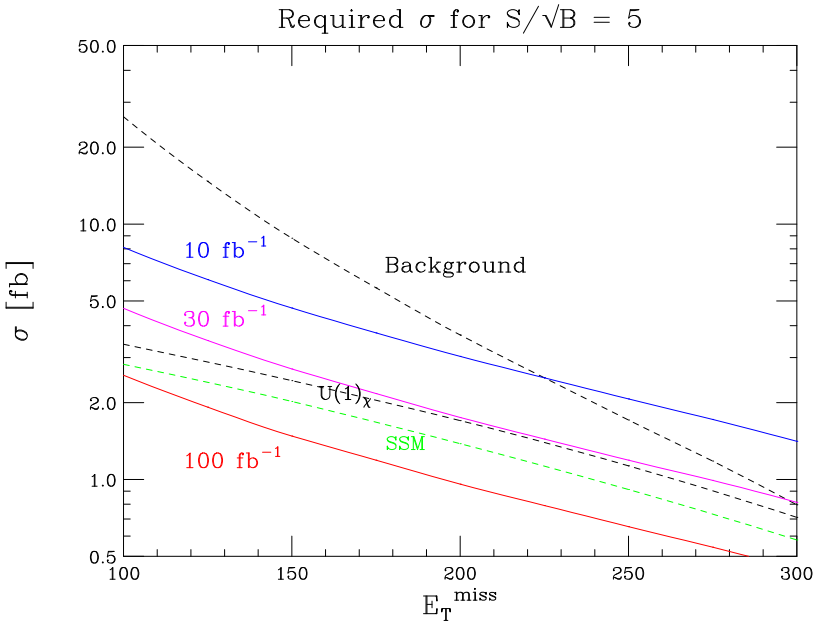

Figure 1: Missing E_T dependence of the SM background and two example Z' models. Included are curves showing the required Z' cross section for $S/\sqrt{B} = 5$ at the LHC for $10\,\text{fb}^{-1}$, $30\,\text{fb}^{-1}$, and $100\,\text{fb}^{-1}$.

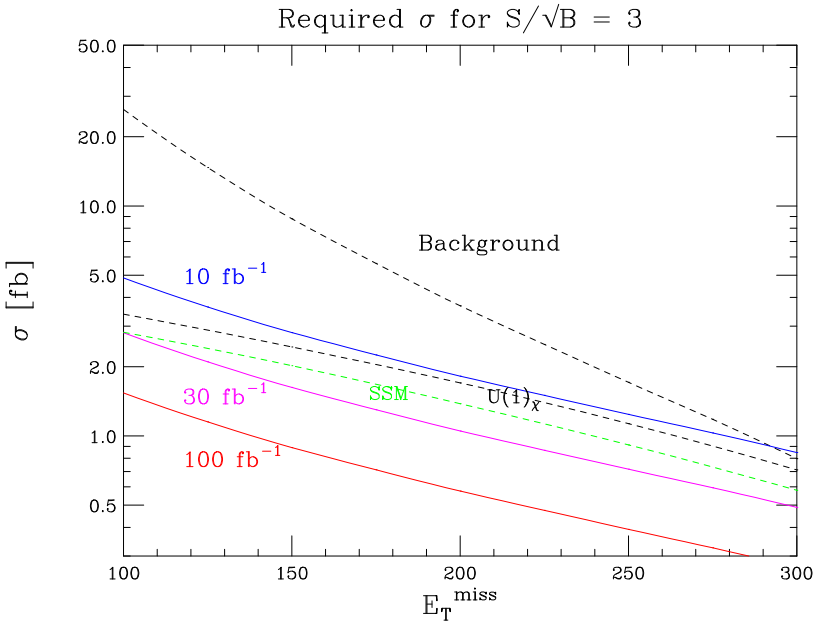

Figure 2: Missing E_T dependence of the SM background and two example Z' models. Included are curves showing the required Z' cross section for $S/\sqrt{B} = 3$ at the LHC for $10\,\text{fb}^{-1}$, $30\,\text{fb}^{-1}$, and $100\,\text{fb}^{-1}$.

decays are accounted for by SM neutrinos only, or whether decays to other exotic states are occuring. Although at first this appears more model-dependent, the matrix element for ZZ' production actually possesses a simple structure that can be encapsulated in a few quantities. Two distinct classes of Feynman diagrams contribute to the process: final-state radiation (FSR) graphs where the Z is emitted from the neutrinos, and initial-state radiation (ISR) graphs where the Z is emitted from the initial quark line. Examples of each type are shown in Fig. (3). We note that because of the invariant mass cut, diagrams where the leptons are emitted from the Z' are numerically negligible. The particle labeled ν in the graphs can denote either a SM neutrino or a hidden sector state. If it is a hidden state, it does not couple to the Z boson and therefore can be produced only via ISR graphs. We have checked that the interference of ISR and FSR contributions is numerically small, indicating that only squared ISR and squared FSR graphs contribute to the signal cross section. This can be partially understood by noting that the Z' propagator cannot be simultaneously on-shell in both types of diagrams, indicating that for narrow states the interference should be suppressed.

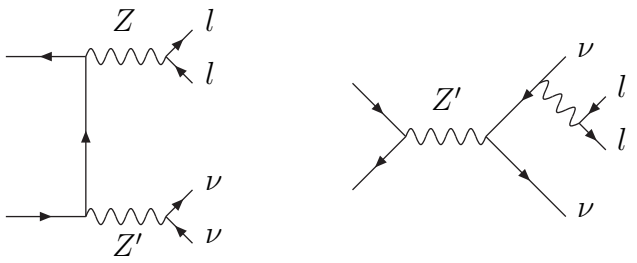

Figure 3: Example initial-state radiation diagram (left) and final-state radiation diagram (right). The particle labeled ν can denote either a SM neutrino or hidden sector state; in the second case, it can only be produced via initial-state radiation.

Generically, an ISR Z will be softer than one from FSR, so that we can expect a corresponding preference for a softer $\not{E}_T$ spectrum from ISR than FSR. This is shown in Fig. (4), where the fraction of the total ISR or FSR cross-section surviving a given $\not{E}_T$ cut is shown. It is seen that the ISR contribution drops off more quickly, as expected. Also shown is the SM background, which drops off more quickly than either Z' contribution.

The relative size of the ISR and FSR contributions determines how well a Z' decaying to hidden sector particles can be extracted. A large ISR contribution implies that non-standard decays can be measured. The simplicity of the matrix element structure allows us to parametrize how different Z' states decay via ISR and FSR contributions in a model independent way. To see this, we first write the cross section subject to the basic acceptance cuts and missing E_T cut as

$$\sigma = \sigma^u_{ISR} + \sigma^d_{ISR} + \sigma^u_{FSR} + \sigma^d_{FSR}, \tag{3.2}$$

where up and down quark contributions have been separated. Each $\sigma^{u,d}_{ISR,FSR}$ can in turn be written as a product of two distinct terms: a piece which incorporates the matrix ele-

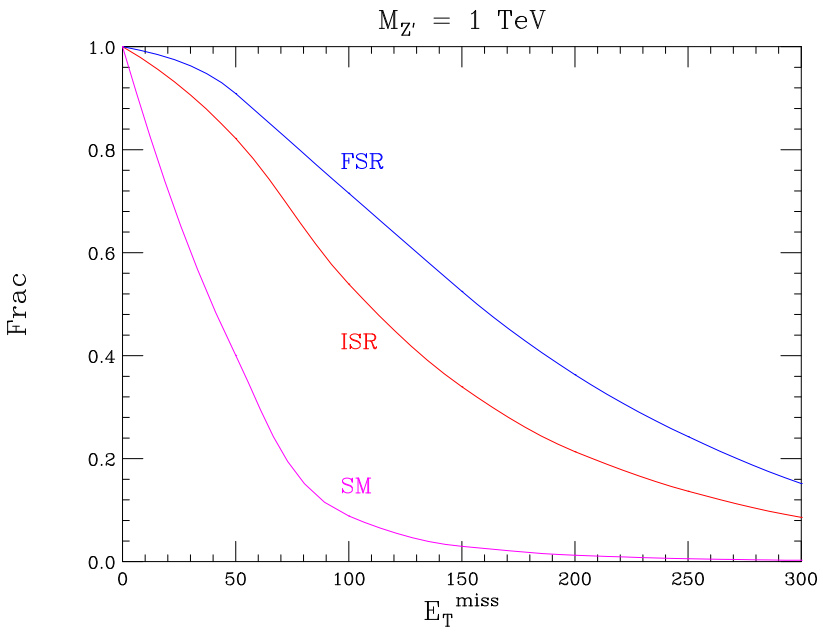

Figure 4: Fractions of ISR, FSR, and SM events which survive a lower missing E_T cut.

ments, parton distribution functions, and experimental cuts, denoted as $f^{u,d}_{ISR,FSR}$; a piece which depends on the charges from a given model, $Q^{u,d}_{ISR,FSR}$. We then have $\sigma^{u,d}_{ISR,FSR} = f^{u,d}_{ISR,FSR} Q^{u,d}_{ISR,FSR}$. The coupling structure of the various terms takes the form

$$Q^q_{ISR} \equiv \left((q'^2_V + q'^2_A)(q^2_V + q^2_A) + 4q'_V q'_A q_V q_A\right) \frac{\Gamma^{inv}_{Z'}}{\Gamma_{Z'}} \tag{3.3}$$

and

$$Q^q_{FSR} \equiv (q'^2_V + q'^2_A)(q^2_V + q^2_A) \frac{\Gamma^{SM\nu}_{Z'}}{\Gamma_{Z'}}, \tag{3.4}$$

where $\Gamma^{SM\nu}_{Z'}$, $\Gamma^{inv}_{Z'}$ denote the partial widths of the Z' to SM ν's or to *any* invisible particle (SM ν's or hidden sector states), and $\Gamma_{Z'}$ is the total width. A prime on a charge indicates that it is a Z' charge, while no prime denotes a SM Z charge. A and V subscripts denote axial and vector charges, respectively. Any Z' model can then be constructed by dialing $Q^{u,d}_{ISR,FSR}$ appropriately. The functions $f^{u,d}_{ISR,FSR}$ depend on the given model under consideration only through the Z' mass in the narrow width approximation.

Values of the Q charges are given in Table (1) for the the sequential Standard Model (SSM) and $U(1)_\chi$ model discussed previously. We also show a $U(1)_B$ model with gauge coupling $g' = 1$ in which the Z' couples to baryon number, and which also includes a hidden sector state, assumed to be a vector-like fermion with unit charge. We present charge values for the SSM and $U(1)_\chi$ models with the same hidden state. The increase of the Q_{ISR} when the hidden state is present can be observed in Table (1). We will see later that the Q values assuming only SM neutrino decays are determined once the Drell-Yan channel

	$U(1)_\chi$	$U(1)_\chi^{hid}$	SSM	SSM^{hid}	$U(1)_B$
Q_u^{FSR}	0.274	0.212	0.292	0.197	0
Q_d^{FSR}	1.75	1.36	0.481	0.324	0
Q_u^{ISR}	0.274	0.589	0.436	1.08	1.49
Q_d^{ISR}	0.432	0.931	0.907	2.26	1.90
u_V	0	0	$\frac{1}{4} - \frac{2}{3}\sin^2\theta_W$	$\frac{1}{4} - \frac{2}{3}\sin^2\theta_W$	$\frac{1}{3}$
u_A	$\frac{1}{2\sqrt{6}}$	$\frac{1}{2\sqrt{6}}$	$\frac{-1}{4}$	$\frac{-1}{4}$	0
d_V	$\frac{-2}{\sqrt{6}}$	$\frac{-2}{\sqrt{6}}$	$\frac{-1}{4} + \frac{1}{3}\sin^2\theta_W$	$\frac{-1}{4} + \frac{1}{3}\sin^2\theta_W$	$\frac{1}{3}$
d_A	$\frac{-1}{\sqrt{6}}$	$\frac{-1}{\sqrt{6}}$	$\frac{1}{4}$	$\frac{1}{4}$	0
e_V	$\frac{2}{\sqrt{6}}$	$\frac{2}{\sqrt{6}}$	$\frac{-1}{4} + \sin^2\theta_W$	$\frac{-1}{4} + \sin^2\theta_W$	0
e_A	$\frac{-1}{\sqrt{6}}$	$\frac{-1}{\sqrt{6}}$	$\frac{1}{4}$	$\frac{1}{4}$	0
X_V	0	1	0	1	1
X_A	0	0	0	0	0

Table 1: Q's for various models, multiplied by 10^3. We have also included the underlying charges of the considered model for orientation, with hidden state charges denoted by X. See the text for further explanation.

$pp \to Z' \to \ell^+\ell^-$ is observed. Measuring different Q values than predicted by Drell-Yan studies would indicate the presence of hidden sector Z' decays. If leptonic Z' decays do not occur, such as in the $U(1)_B$ model, the $pp \to ZZ' \to \ell^+\ell^- \not{E}_T$ process considered here becomes a discovery channel.

To develop some intuition, we present below several plots showing features of the cross section for different Q choices. For simplicity of presentation we make the simplifying assumption $Q^u_{FSR} = Q^d_{FSR} = Q_{FSR}$ and $Q^u_{ISR} = Q^d_{ISR} = Q_{ISR}$. The degeneracy between $Q^u_{ISR,FSR}$ and $Q^d_{ISR,FSR}$ in the plots can be broken by utlizing the information $f^u_{ISR} = 353$ fb, $f^d_{ISR} = 227$ fb, $f^u_{FSR} = 2.71$ pb, $f^d_{FSR} = 1.40$ pb, evaluated for a missing E_T cut of 150 GeV. We note that the kinematic dependences of the u and d-quark cross sections on the missing E_T cut are very similar. We focus on three example cases: $Q_{FSR} = Q_{ISR} = 10^{-3}$; $Q_{FSR} = 10^{-4}$ and $Q_{ISR} = 10^{-3}$; $Q_{FSR} = 10^{-4}$ and $Q_{ISR} = 5 \times 10^{-3}$. These values are roughly consistent with those present in typical models as shown in Table (1). We show in Fig. (5) the ISR fraction of the total cross section as a function of the missing E_T cut for $M_{Z'} = 1$ TeV. For $Q_{FSR} = Q_{ISR}$, the ISR fraction of the cross section is less than 20%. The FSR matrix elements give a larger contribution to the cross section, suggesting that it will be difficult to dig out the hidden sector sector component from invisible decays. We will quantify this further later. The cross sections for the Q charges under consideration are shown in Fig. (6). For comparison, we overlay the curves showing the required cross sections for $S/\sqrt{B} = 3, 5$ with 100 fb^{-1} from Figs. (1) and (2). We see that at least $S/\sqrt{B} = 3$ evidence is possible at the LHC for a range of Q values.

To study what Z' masses can be probed, we show in Fig. (7) the Z' cross section as a function of mass for several different example Q values. Since the masses are larger, the corresponding Q values needed for observation are larger, so we present results assuming

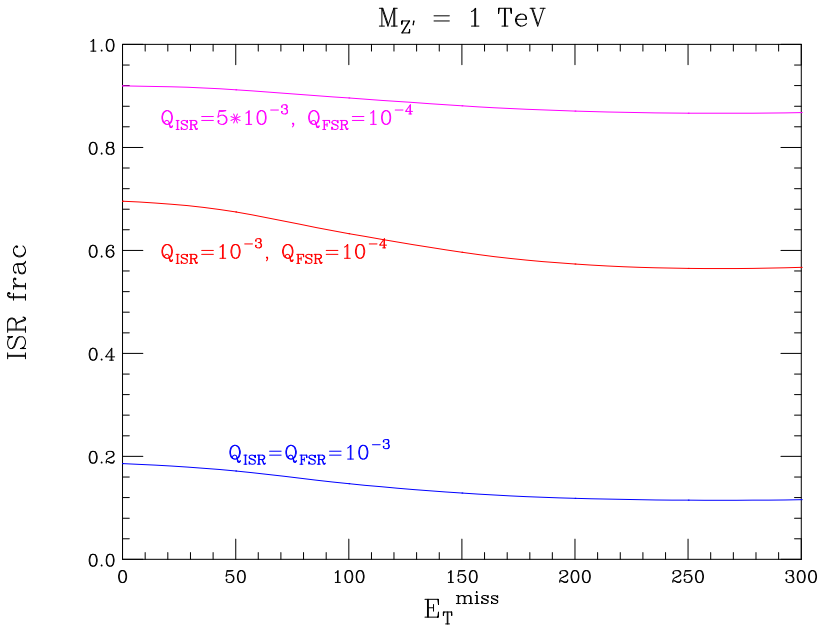

Figure 5: Fraction of cross section coming from ISR initiated diagrams as a function of missing E_T cut for three example Q choices.

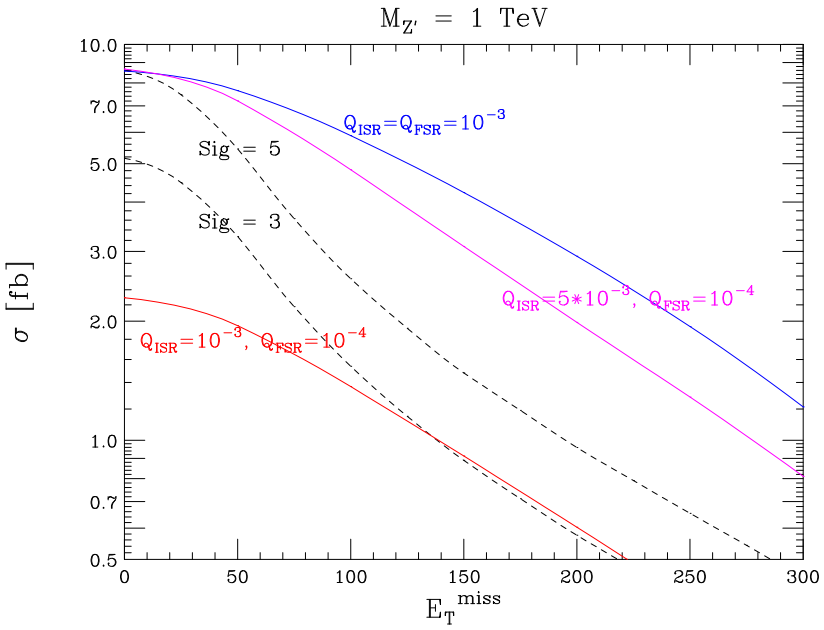

Figure 6: Cross section as a function of missing E_T cut for three example Q choices. The cross sections required for $S/\sqrt{B} = 3, 5$ assuming 100 fb^{-1} are shown as dashed lines.

somewhat larger charges. We show the results for missing E_T cuts of both 150 and 200 GeV; the value that actually maximizes $S/\sqrt{B}$ varies with $M_{Z'}$. Included in this plot are the required cross sections for $S/\sqrt{B} = 3, 5$ assuming 100 fb^{-1}. For $Q_{FSR} = 5 \times 10^{-3}$, masses beyond 2 TeV are easily observable. If $Q_{FSR} = 10^{-4}$ and the ISR charge is larger, the case relevant for Z' decays to hidden sectors, only masses up to 1.25 or 1.5 TeV can be probed with $S/\sqrt{B} = 5$.

Finally, if the Z' does not decay into leptons but does decay to hidden sector states, $pp \to ZZ' \to \ell^+\ell^- \not{E}_T$ becomes a discovery channel. The experimental search for this leptophobic Z' will proceed by moving upward a minimum missing E_T cut and looking for a signal to emerge. The shape of the $\not{E}_T$ spectrum should give some sensitivity to the Z' mass. Also, if a more complicated structure of new physics than a simple isolated Z' is discovered, we will want to determine whether the $\ell^+\ell^- \not{E}_T$ signal arises from a single new gauge boson or multiple states.

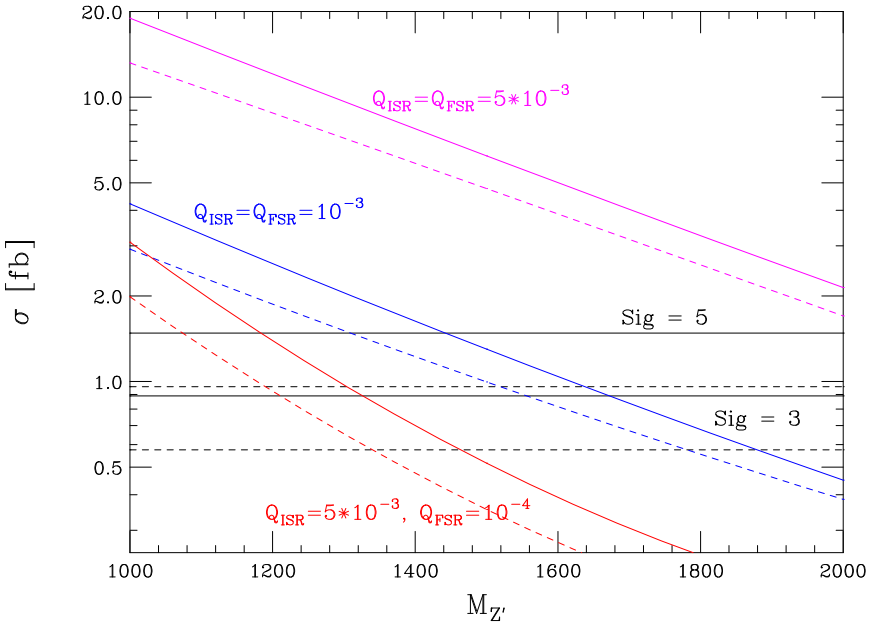

Figure 7: The Z' cross section as a function of mass for several different example Q values. The solid lines assume a cut $\not{E}_T > 150$ GeV, the dashed lines assume $\not{E}_T > 200$ GeV. The horizontal lines are the cross sections required for $S/\sqrt{B} = 3, 5$ with 100 fb^{-1}; again, solid lines assume $\not{E}_T > 150$ GeV and dashed lines assume $\not{E}_T > 200$ GeV. The mass reach for a given missing E_T cut and signifance is determined by finding the appropriate intersection of curve and horizontal line.

We determine the statistical measurement error for three fiducial Z' masses, 1, 1.5, and 2 TeV, by performing a χ^2 comparison of their missing E_T spectra versus other masses. We set $Q_{FSR} = 0$ to simulate a completely leptophobic Z' for our spectra. The cross section is divided into several bins in missing E_T; we take the ratio of each bin to the total rate surviving the $\not{E}_T > 150$ cut to normalize. We generate $\not{E}_T$ templates for many other masses

and compare the ratios in each bin to the ratios for each fiducial mass, and determine for what masses a total 1 σ deviation is exceeded in each case; this occurs when the total χ^2 reaches 1. In Fig. (8) we have plotted 1 σ error bands for the three Z' masses as a function of hidden cross section after the missing E_T cut of 150 GeV, for the SLHC luminosity of 1 ab^{-1}. We have not taken into account errors other than statistical, such as PDF uncertainties; we leave the inclusion of such errors for a more complete analysis. One can see, however, that given just the statistical error, there is good sensitivity to the mass given a sufficiently large cross section (reasonable for a leptophobic Z') and sufficient integrated luminosity. For reference, a 1 fb, $\not{E}_T > 150$ cross section corresponds to $Q^u_{ISR} = Q^d_{ISR}$ values of 0.00172, 0.0123, and 0.0377, for masses of 1 TeV, 1.5 TeV, and 2 TeV, respectively.

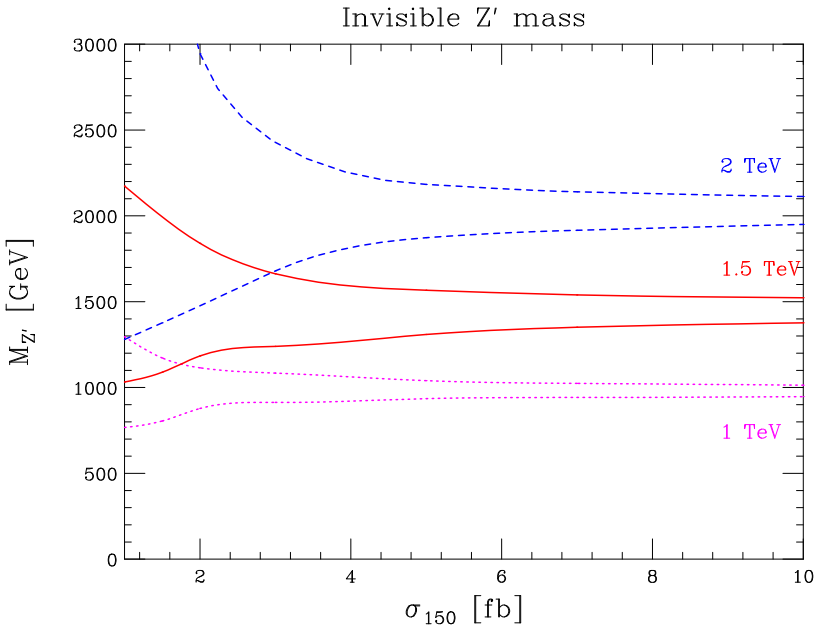

Figure 8: 1σ statistical error bands on Z' mass measurement, given hypotheses of $M_{Z'} = 1, 1.5, 2$ TeV, as a function of the total cross-section $pp \to ZZ' \to \ell^+\ell^- \not{E}_T$ with $\not{E}_T > 150$ GeV.

4 Finding the hidden sector

We wish to study whether LHC results can determine if invisible Z' decays occur only to SM neutrinos, or whether other states are involved. This would provide insight into possible hidden sectors to which the Z' couples.

The crucial fact that allows this measurement to be performed is that the charges Q introduced in the previous section are predicted by the analysis of Drell-Yan Z' production in [8] if the Z' decays invisibly only to neutrinos. We note that

$$Q^q_{ISR} = \left(\frac{c_q}{2} \frac{C}{C+1} (q_V^2 + q_A^2) + e_q \frac{C}{C-1} q_V q_A \right) \frac{\Gamma^{inv}_{Z'}}{\Gamma^{\nu}_{Z'}}, \tag{4.5}$$

and

$$Q^q_{FSR} = \frac{c_q}{2}\frac{C}{C+1}(q_V^2 + q_A^2), \tag{4.6}$$

where c_q and e_q are the on-peak couplings determined in [8]:

$$\begin{aligned} c_q &= \frac{M_{Z'}}{24\pi\Gamma}(q_R'^2 + q_L'^2)(l_R'^2 + l_L'^2); \\ e_q &= \frac{M_{Z'}}{24\pi\Gamma}(q_R'^2 - q_L'^2)(l_R'^2 - l_L'^2); \\ C &= \frac{l_L'^2}{l_R'^2} = \frac{c_u + e_u - c_d - e_d}{c_u - e_u - c_d + e_d}. \end{aligned} \tag{4.7}$$

Q^q_{FSR} is fixed by c_q and e_q. If the Z' decays invisibly only to neutrinos, then $\Gamma^{inv}_{Z'} = \Gamma^{\nu}_{Z'}$; Q^q_{ISR} is then completely predicted by the on-peak couplings. Any deviation of Q^q_{ISR} from this limit indicates additional invisible decays of the Z'.

We first determine how big an excess over the expected invisible cross section predicted by on-peak data can be observed. In addition to SM production of leptons and missing energy, the signal $pp \to ZZ' \to \ell^+\ell^-\nu_\ell\bar{\nu}_\ell$ now becomes a background to $pp \to ZZ' \to \ell^+\ell^- X\bar{X}$, where the Xs are the hidden sector particles. In Fig. (9) we show the the size of the excess cross section over that predicted by the on-peak data which can be excluded at 95% C.L. for 100 fb^{-1} and 1000 fb^{-1} of data; as this is a difficult measurement we have assumed a sizeable amount of integrated luminosity. The excess cross section for which 3σ evidence can be obtained is shown in Fig. (10). We have used a cut of $\not{E}_T > 200$ GeV in producing these numbers. The excess cross section that can be probed depends crucially on how well the expected invisible cross section can be predicted from on-peak data. To determine this precision, the expected errors on c_q, e_q from [8] must be propagated through the expressions in Eqs. (4.5) and (4.6). We present results for fractional errors on the predicted invisible cross section of 10% and 25%, which are consistent with the error propagation, as well as for the idealized limit of no error. From Figs. (6) and (7), we see that cross sections for typical Q values with $\not{E}_T > 200$ GeV are between 1-10 fb. Using the 10% error curve from Fig. (9), hidden sector decays leading to excess cross sections of 1-2 fb can be excluded at 95% confidence level. If no on-peak cross section is observed, then the left side of Figs. (9) and (10) indicate how well completely invisibly decaying Z' bosons can be probed. Completely invisibly decaying Z' boson cross sections can be excluded down to 0.5 fb given sufficient integrated luminosity.

Several reductions of the error associated with the invisible cross section prediction are possible. With 100 fb^{-1} the error comes mostly from parton distribution functions; with 1000 fb^{-1} it comes entirely from parton distribution functions. These uncertainties will be significantly improved with LHC data. In addition, one may be able to normalize the FSR contribution to on-peak data, due to the similar PDF and coupling structure. Approaching a 5% error is not inconceivable.

We now interpret this excess cross section using our effective charges. We write $Q^{u,d}_{ISR} = Q^{u,d}_{SM\nu} + Q^{u,d}_{hid}$, where $Q_{SM\nu}$ can be predicted from the on-peak data and $Q^{u,d}_{hid}$ is the portion

coming from decays to hidden sector states. We plot in Fig. (11) the size of this excess cross section as a function of Q_{hid}, where $Q^u_{hid} = Q^d_{hid}$. Using this graph and keeping in mind the 1-2 fb cross sections, we observe that it will be difficult to significantly constrain hidden sector decays if $M_{Z'}$ is significantly greater than 1 TeV. For a 1 TeV state, charges in the range $Q^q_{hid} \geq 5 \times 10^{-3}$ can be probed.

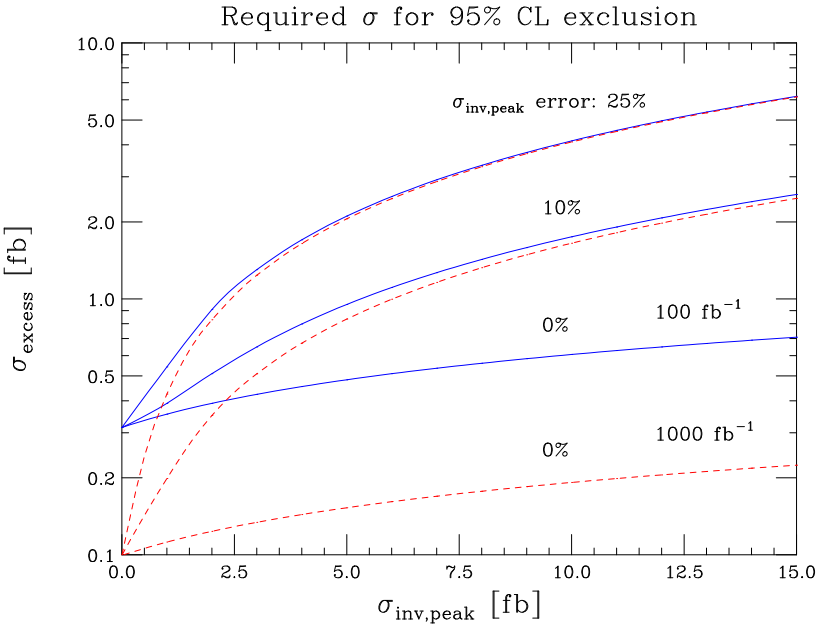

Figure 9: Excess cross section over that predicted by on-peak data, σ^{peak}_{inv}, which can be excluded at 95% confidence level for 100 fb^{-1} and 1000 fb^{-1}. Errors on the predicted σ^{peak}_{inv} of 0%, 10% and 25% from on-peak data are assumed. σ_{excess} results from decays to hidden sector particles.

Although the 95% confidence level and 3σ reaches in the $Q - M_{Z'}$ plane can be determined from Figs. (6), (7), (9), (10), and (11), since the parameter space is large and the graphs are numerous, we summarize below several canonical cases.

- 95% exclusion for pure hidden sector Z': From Fig. (9), the required cross sections to exclude this state are $\sigma_{excess} > 0.3$ fb with 100 fb^{-1} and $\sigma_{excess} > 0.1$ fb with 1000 fb^{-1}. This implies the following exclusion limits for fixed $M_{Z'}$, Q_{hid}.
  - $M_{Z'} = 1$ TeV: $Q_{hid} < 2 \times 10^{-3}$ with 100 fb^{-1} and $Q_{hid} < 5 \times 10^{-4}$ with 1000 fb^{-1} using Fig. (11).
  - $Q_{hid} = 5 \times 10^{-3}$: $M_{Z'} > 1300$ GeV with 100 fb^{-1} and $M_{Z'} > 1700$ GeV with 1000 fb^{-1} using Fig. (7).
- Z' boson with $M_{Z'} = 1$ TeV, $Q_{ISR} = 5 \times 10^{-3}$, $Q_{FSR} = 10^{-4}$: We assume a 10% error in the invisible cross section prediction when interpreting this state. Using the graphs in a similar fashion as above, the following information about Q_{hid} can be obtained.

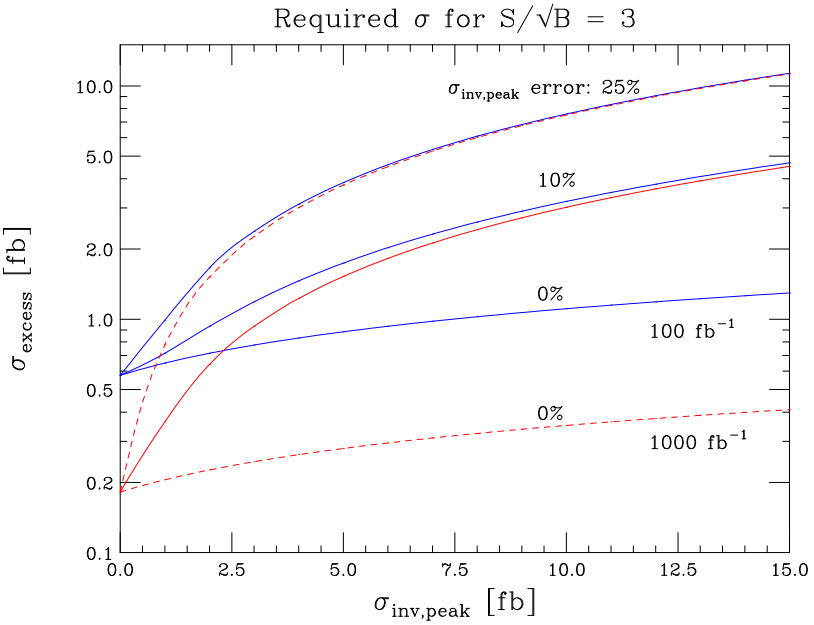

Figure 10: Excess cross section over that predicted by on-peak data, σ_{inv}^{peak}, which can be observed at 3σ for 100 fb^{-1} and 1000 fb^{-1}. Errors on the predicted σ_{inv}^{peak} of 0%, 10% and 25% from on-peak data are assumed.

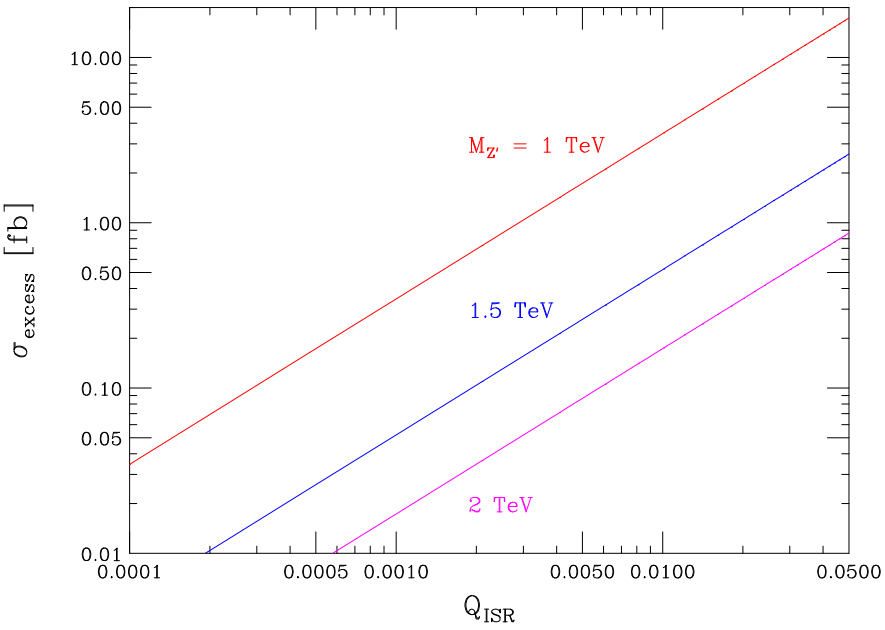

Figure 11: Excess cross section σ_{excess} as a function of $Q_{ISR}^{u,d} = Q_{ISR}$.

- *95% exclusion*: $Q_{hid} < 2 \times 10^{-3}$ with $100\,\text{fb}^{-1}$ and $Q_{hid} < 10^{-3}$ with $1000\,\text{fb}^{-1}$.
- 3σ *evidence*: can probe $Q_{hid} = 4 \times 10^{-3}$ with $100\,\text{fb}^{-1}$ and $Q_{hid} = 2 \times 10^{-3}$ with $1000\,\text{fb}^{-1}$.

5 Conclusions

We have studied the feasibility of observing an invisible Z' through the process $pp \to ZZ' \to \ell^+\ell^- XX^\dagger$ at the LHC, where X is any neutral, (quasi-) stable state. We found that 3σ evidence of this process could be made with as little as 10 fb^{-1} of data for a standard 1 TeV $U(1)_\chi$ Z' with gauge coupling $g' = 1$, while a 5σ discovery is possible with 30 fb^{-1}. With our results, using Figs. (6-7) in conjunction with Figs. (1-2), the discovery reach of LHC for observing any invisibly decaying Z' can be computed. We parametrized our results in terms of two effective charges that completely describe production of a Z' in conjunction with a Z radiated off the initial state (ISR) or the final state (FSR). We found that for a 1 TeV Z', any model with $Q_{ISR} > 10^{-3}$, $Q_{FSR} > 10^{-4}$ can be observed at 3σ with 100 fb^{-1} of data. This shows that a leptophobic Z' that cannot be observed through the usual Drell-Yan channel at the LHC can be discovered if it decays invisibly to hidden sector states. We showed that some sensitivity to the Z' mass can be obtained by studying the missing E_T spectrum.

In addition, we demonstrated that an excess invisible decay of the Z' to hidden sector states over the predicted cross section for $pp \to ZZ' \to \ell^+\ell^-\bar{\nu}\nu$ from on-peak data can be excluded at 95% confidence level if the size of this cross section is 20-30% of the total cross section, given a 10% error on the predicted invisible cross section. The exotic states may, for example, be dark states from a "Hidden Valley" model [12]. The Z' may be a communicator to a light hidden sector with MeV mass dark matter states as in the model of [13]; this is motivated by the INTEGRAL/SPI observation [21] of a 511 keV line toward the galactic center. To get 20-30% of the invisible cross section of the Z' from hidden decays will require in most cases a hidden sector with multiple states to compete with the SM neutrino invisible decays. In particular, when $Q_{ISR} \simeq Q_{FSR}$, the branching fraction to new hidden sector states must be approximately the same as the branching fraction to SM neutrinos in order to obtain a $\sim 20\%$ deviation in the invisible cross section $pp \to ZZ' \to \ell^+\ell^- XX^\dagger$ predicted from on-peak data. This is on account of the hidden sector states entering only through graphs where the Z is radiated off the initial state quark lines; these initial state graphs usually compose a relatively small fraction of the total cross section: $\sim 20\%$ from Fig. (5) for the fiducial case of the effective charges for initial state and final state Z radiation being roughly the same. Despite this potential difficulty of observing decays to hidden sector states, we have shown that it is nonetheless feasible, given the presence of such a hidden sector. The possibility to observe such dark states through the hidden decays of a new vector gauge boson makes the accurate measurement of the invisible Z' at the LHC an exciting and reachable goal.

Acknowledgments

The authors are supported by the DOE grant DE-FG02-95ER40896, Outstanding Junior Investigator Award, by the University of Wisconsin Research Committee with funds provided by the Wisconsin Alumni Research Foundation, and by the Alfred P. Sloan Foundation.

References

[1] For a review, see R. N. Mohapatra, *Unification and Supersymmetry*, Springer, New York, 1986.

[2] For a review, see J. L. Hewett and T. G. Rizzo, Phys. Rept. **183**, 193 (1989).

[3] For a review, see J. L. Hewett and M. Spiropulu, Ann. Rev. Nucl. Part. Sci. **52**, 397 (2002) [arXiv:hep-ph/0205106].

[4] For a review, see M. Schmaltz and D. Tucker-Smith, Ann. Rev. Nucl. Part. Sci. **55**, 229 (2005) [arXiv:hep-ph/0502182].

[5] T. Aaltonen *et al.* [CDF Collaboration], Phys. Rev. Lett. **99**, 171802 (2007) [arXiv:0707.2524 [hep-ex]]; R. J. Hooper [D0 Collaboration], Int. J. Mod. Phys. A **20**, 3277 (2005).

[6] The relevant studies can be found in the ATLAS and CMS technical design reports, available at http://atlas.web.cern.ch/Atlas/GROUPS/PHYSICS/TDR/access.html; https://cmsdoc.cern.ch/cms/cpt/tdr/.

[7] Several excellent reviews of Z' physics that contain discussions of measuring couplings at colliders and list original references are M. Cvetic and S. Godfrey, arXiv:hep-ph/9504216; A. Leike, Phys. Rept. **317**, 143 (1999) [arXiv:hep-ph/9805494]; T. G. Rizzo, arXiv:hep-ph/0610104; P. Langacker, arXiv:0801.1345 [hep-ph].

[8] F. Petriello and S. Quackenbush, arXiv:0801.4389 [hep-ph].

[9] C. Coriano, A. E. Faraggi, M. Guzzi arXiv:0802.1792 [hep-ph]

[10] K. Gumus, N. Akchurin, S. Esen and R.M. Harris, CMS Note 2006/070; S. Gonzalez de la Hoz,L. March and E. Roos, ATL-PHYS-PUB-2006-003.

[11] For a review, see D. J. H. Chung, L. L. Everett, G. L. Kane, S. F. King, J. D. Lykken and L. T. Wang, Phys. Rept. **407**, 1 (2005) [arXiv:hep-ph/0312378]; for a recent example see P. Langacker, G. Paz, L. T. Wang and I. Yavin, Phys. Rev. Lett. **100**, 041802 (2008) [arXiv:0710.1632 [hep-ph]].

[12] M. J. Strassler and K. M. Zurek, Phys. Lett. B **651**, 374 (2007) [arXiv:hep-ph/0604261]. M. J. Strassler and K. M. Zurek, Phys. Lett. B **661**, 263 (2008) [arXiv:hep-ph/0605193].

[13] D. Hooper and K. M. Zurek, arXiv:0801.3686 [hep-ph].

[14] K. Cheung and T. C. Yuan, JHEP **0703**, 120 (2007) [arXiv:hep-ph/0701107]

[15] S. G. Frederiksen, N. Johnson, G. L. Kane and J. Reid, Phys. Rev. D **50**, 4244 (1994); D. Choudhury and D. P. Roy, Phys. Lett. B **322**, 368 (1994) [arXiv:hep-ph/9312347]; S. P. Martin and J. D. Wells, Phys. Rev. D **60**, 035006 (1999) [arXiv:hep-ph/9903259]; R. M. Godbole, M. Guchait, K. Mazumdar, S. Moretti and D. P. Roy, Phys. Lett. B **571**, 184 (2003) [arXiv:hep-ph/0304137].; H. Davoudiasl, T. Han and H. E. Logan, Phys. Rev. D **71**, 115007 (2005) [arXiv:hep-ph/0412269].

[16] H. Davoudiasl, T. Han and H. E. Logan, Phys. Rev. D **71**, 115007 (2005) [arXiv:hep-ph/0412269].

[17] F. Maltoni and T. Stelzer, JHEP **0302**, 027 (2003) [arXiv:hep-ph/0208156].

[18] T. Sjostrand, S. Mrenna and P. Skands, JHEP **0605**, 026 (2006) [arXiv:hep-ph/0603175].

[19] J. Ohnemus and J. F. Owens, Phys. Rev. D **43**, 3626 (1991); S. Frixione, Nucl. Phys. B **410**, 280 (1993).

[20] M. Dittmar, F. Pauss and D. Zurcher, Phys. Rev. D **56**, 7284 (1997) [arXiv:hep-ex/9705004].

[21] P. Jean *et al.*, Astron. Astrophys. **407**, L55 (2003) [arXiv:astro-ph/0309484]. G. Weidenspointner *et al.*, Nature **451**, 159 (2008).